This is a repository copy of *Turbulent burning rates of gasoline components, Part 1-Effect of fuel structure of C-6 hydrocarbons*.

White Rose Research Online URL for this paper:
http://eprints.whiterose.ac.uk/94056/

Version: Accepted Version

Turbulent Burning Rates of Gasoline Components, Part 1 - Effect of Fuel Structure of C_6 Hydrocarbons

A.A. Burluka[a], R.G. Gaughan[b], J.F. Griffiths[c], C. Mandilas[a,*], C.G.W. Sheppard[a], R. Woolley[d]

[a] School of Mechanical Engineering, The University of Leeds, Leeds LS2 9JT, UK

[b] ExxonMobil Research and Engineering Company, Paulsboro Technical Center, 600 Billingsport Road, Paulsboro, NJ 08066, United States

[c] School of Chemistry, University of Leeds, Leeds, LS2 9JT, United Kingdom

[d] The University of Sheffield, Department of Mechanical Engineering, Mappin Street, S1 3JD, UK

[*] Corresponding author. Present address: The Centre for Research and Technology, Hellas, Chemical Process & Energy Resources Institute, 3km Charilaou-Thermi Road, Thermi 57001, Greece, mandilas@cperi.certh.gr

Abstract

Measurements of laminar and turbulent burning velocities have been made for premixed hydrocarbon-air flames with six carbon atoms including unsaturated, branched and cyclic molecules. The seven different fuels studied were n-hexane, 1-hexene, 1-hexyne, 2,2 dimethyl butane, 2 methyl pentane (isohexane), cyclohexane and cyclohexene. The tests were performed in a constant volume, optically accessed spherical bomb, with the use of the schlieren technique and a high-speed camera. The deflagrations were initiated at elevated pressure and temperature of 0.5 MPa and 360 K, where burning velocity data is relatively sparse, under laminar and turbulent conditions with rms turbulent velocities of 2 and 6 m/s and for equivalence ratios of 0.78 to 1.67. The primary objective of this work was to compare the turbulent burn rates of the different fuel-air mixtures; the laminar burning velocities were used to interpret the turbulent data. The ranking of the laminar burning velocity was overall found to be 1-hexyne > cyclohexene > 1-hexene > cyclohexane > n-hexane > 2-methyl pentane > 2,2 dimethyl butane for the range of equivalence ratios tested. The ranking was found to be the same for the turbulent burn rate measurements, particularly so for the slowest and fastest fuels. As the rms turbulent velocity increased the relative differences between the fuels were found to generally increase for lean mixtures, remain similar around stoichiometric equivalence ratio and decrease for rich mixtures. This behaviour was linked to the sensitivity of turbulent flames to stretch and thermo-diffusive stability.

Keywords: laminar flames, turbulent flames, burning velocity, hydrocarbon combustion

1. Introduction

Burning velocity has been the subject of numerous experimental and theoretical investigations spanning many decades, prompted to an extent by an interest in its effect on the performance of internal combustion engines. Burn rate affects engine performance, efficiency and cycle-to-cycle variability [1]. Thus, understanding the factors that influence the burn rate enables better control of engine combustion quality and emissions. The rate of combustion in an engine is a function of the turbulent burning velocity, which is itself a function of the physico-chemical features of a fuel-air mixture encapsulated in its laminar burning velocity, u_l, and the turbulence characteristics of the flow field within the engine. The influence of fuel structure on the laminar burning velocity has been reported [e.g. 2-6]. However, published data on the influence of hydrocarbon molecular structure on burn rate under turbulent conditions and initial flame pressures relevant to those in engines is extremely sparse. Consequently, the primary aim of the current work was to investigate the effects of fuel structure and equivalence ratio, ϕ, on the turbulent burn rate of spark-initiated growing flames, at elevated initial temperature and pressure.

Presented in this paper are experimentally determined turbulent and laminar burn rates for a set of hydrocarbons of varied structure, but all with 6 carbon atoms: 2,2-dimethyl butane, 2-methyl pentane n-hexane, cyclohexane, 1-hexene, cyclohexene and 1-hexyne. These fuels, with the exception of 1-hexyne, are representative components of automotive gasoline blends. Diagrams showing the molecular structures, bond energies, heat of formation and molar mass of the fuels studied are depicted in Table 1.

The turbulent burning velocity, u_t, is primarily a function of the turbulent velocity within the fluid. Stemming from classical works of Damköhler, a common expression for turbulent burn rate is:

$$\frac{u_t}{u_l} \sim \frac{u'}{u_l} \cdot f\left(\frac{\tau}{t_f}\right) \qquad (1)$$

where u' is the rms turbulent velocity and f is a function of the ratio of the turbulent timescale, τ, to the characteristic time of reactions within the flame, t_f, known as the Damköhler number, Da. It has long been established that the laminar burn rate is strongly dependent on fuel type, thus, fuel properties must also have an influence on u_t. Work performed here focused on the influence of fuel structure on u_t. The effects on burn rate were examined for equivalence ratios of 0.78 to 1.67, at two rms turbulent velocities, $u' = 2$ and 6 m/s. These conditions were chosen as they reflect realistic levels of turbulence in engines, where u' near the top dead centre is about half the piston speed (e.g. $u' = 5$ m/s, for 75 mm stroke, at 4000 rpm [1]) and typically an order of magnitude greater than u_l.

This paper is the first of a two part study. In Part 2 [8], laminar and turbulent burn rates were obtained for alkanes, n-pentane to n-octane. The two parts of the work were separated as they examine the impact of different aspects of fuel structure on premixed laminar and turbulent burn rates. In this part, the fuels have different fuel structure and bonding, but similar fuel transport properties, whilst in Part 2 the fuels have different chain length and transport properties, but similar straight chain structure.

2. Experimental Procedure and Results Processing

The Leeds MkII spherical bomb operating under laminar and turbulent conditions, was employed for the studies. The effects on burn rate for two different turbulent rms velocities were examined ($u' = 2$ m/s and 6 m/s). Included below is a brief description of the experimental equipment and procedure; more detail is available in references

[9-10]. All experiments incorporated schlieren-based imaging and pressure measurements to enable comparison of burn rate trends at early (constant pressure) and later (pressure rise in the vessel) stages of flame development. Although minor differences were evident, the general trends in burning velocity noted from the schlieren and pressure based results were similar. Hence, for brevity, reported here are only the results derived from the schlieren imaging of the flames.

A schematic diagram of the schlieren system is shown in Figure 1. The light source was a 20 W tungsten element lamp. A condenser lens was positioned at a distance equal to its focal length of 50 mm from the lamp. The light passing through this lens was focused onto an iris, which was used to provide a single point light source. The expanding light beam was focused into a parallel beam using a 150 mm plane convex lens (f-1000) and was passed through the bomb window. On the other side of the vessel, another 150 mm convex plane lens (f-500) of focal length 500 mm was used to focus the light onto a pinhole of 1 mm in diameter, which was used as the knife edge. The light beam passing through the pinhole was focused onto the camera chip. Centrally ignited propagating flames were imaged to the window diameter of 150 mm, using a Photosonics Phantom 9 high speed digital camera with Complementary Metal Oxide Semiconductor (CMOS) chip. Laminar flames were recorded at 2000 frames/s. Turbulent flames were imaged at rates of 6300 and 9000 frames/s, for $u' = 2$ and 6 m/s, respectively.

Mixtures were prepared in the vessel. After each experiment the vessel was flushed several times with compressed air and evacuated. Dry cylinder air was provided for the combustible mixture. Pre- calculated volumes of liquid fuels were injected into the vessel using a gas tight syringe. The fans were ran during mixture preparation, both to ensure full mixing and to assist heat transfer from the vessel's 2 kW electrical heater

positioned close to a wall. For laminar studies the fans were switched off for a period of 60 seconds, following mixture preparation, before ignition. In turbulent tests the fans were maintained at the speed required to produce the desired rms turbulence intensity throughout the mixture preparation, ignition and combustion period. The mixture temperature before ignition was measured using a 1.5 mm K-type stainless steel thermocouple situated inside the vessel.

Deflagrations were initiated at a nominal initial temperature of $T_i = 360$ K and pressure of $P_i = 0.5$ MPa, where published experimental data are relatively sparse, as most information available in the literature is for 0.1 MPa. The relatively high initial temperature ensured complete fuel vaporisation and contributed to the avoidance of condensation on the walls and windows after ignition, while the elevated initial pressure was adopted to provide conditions representative of combustion relevant to internal combustion engines. In the early stages of combustion, for flames of mean flame radius less than the window diameter, pressure and associated unburned gas temperature remained close to the initial values (since mixture volume fraction burned at that radius was less than 4%, with associated mass fraction burned less than 1%). Final bomb pressures were ~3.5 MPa, (for a typical burned to unburned gas expansion ratio of $\rho_b / \rho_u \sim 7.0$). Experiments were conducted for lean ($\phi = 0.78$) to rich ($\phi = 1.67$) conditions.

At least two laminar and five turbulent deflagrations were performed at each condition. For laminar flames, the repeatability tolerance was set at a maximum of 2% in the time elapsed from ignition required to reach a pressure of 0.75 MPa for tests conducted on the same day; and 3% for tests conducted on different days. Turbulent tests exhibited inherent shot-to-shot variability and, hence, a similar tolerance approach could not be followed; typical experimental scatter in burn rate for turbulent

flames was circa 10% (in coefficient of variance, COV), independent of the rms turbulent velocity.

The laminar burning velocity was obtained using what has become a typical method for its determination from spherically expanding flames. Image processing was applied to identify the burned gas area; assuming a spherical flame, the projected flame area, A, was found by converting the schlieren images into binary black (unburned) and white (burned) regions. Image binarisation was achieved in MATLAB via adaptive moving threshold. The main processing steps involved during image manipulation are highlighted in Figure 2. Initially all images (a, b) of a flame movie were rotated to transfer the spark plug probe to the top (c, d). Next, the pre-ignition image was subtracted from the current flame image (e). The subtracted image was binarised (f) before adding it to the pre-ignition grayed image. The combined image (g) was used to find the edges of the spark plug probe protruding into the flame (h). The final step involved filtering of noise around the flame image (red circled areas in image 'g') using a version of the 'bwconncomp' MATLAB function and filling of the spark plug gap to acquire the finalised image (i) with which to obtain the flame area.

The schlieren edge represents an isotherm of circa T_i + 5 K [10] and the cold front flame radius, r_u, is:

$$r_u = r_{sch} + 1.95\,\delta_l \left(\frac{\rho_u}{\rho_b} \right)^{0.5} \qquad (2)$$

here, r_{sch} is the schlieren radius, ρ_u is the density of the reactants and ρ_b is the density of the products. The laminar flame thickness was defined as,

$$\delta_l = \frac{v}{u_l} \qquad (3)$$

where u_l is the stretch-free burning velocity and v is the kinematic viscosity of the reactants. The flame speed, S_n, was found by differentiating cold front flame radius with time,

$$S_n = \frac{dr_u}{dt} \tag{4}$$

The stretch rate of the flame determined using,

$$\alpha = \frac{1}{A}\frac{dA}{dt} = \frac{1}{4\pi r_u^2}\frac{d(4\pi r_u^2)}{dt} = \frac{2}{r_u}S_n \tag{5}$$

The stretch-free flame speed is given by the corresponding stretched flame speed in the linear form,

$$S_s - S_n = L_b\,\alpha \tag{6}$$

As the flame radius increases, the total stretch rate approaches zero so that $S_n \rightarrow S_s$, and that the stretched burn rate, $u_n \rightarrow u_l$. The burnt Markstein length, L_b, is the slope and S_s is the y-axis intercept. The Markstein length of a flame is a physico-chemical flame parameter, customarily used to characterise the effect of stretch rate on flame speed [11]. Positive values of L_b indicate that as the flame expands, and becomes increasingly less stretched, there is a gain in flame speed; the opposite is true for flames with negative L_b. Applying mass conservation, the stretch-free burning velocity is related to S_s by

$$u_l = S_s\frac{\rho_b}{\rho_u} \tag{7}$$

A non-linear variation of flame speed with stretch has also been derived [12],

$$\left(\frac{S_n}{S_s}\right)^2 \ln\left(\frac{S_n}{S_s}\right)^2 = -\frac{2L_b\alpha}{S_s} \tag{8}$$

This was compared to the linear results from Eq. 6 and the differences were found to be typically within 2%. It must be noted that Eqs. 6 and 7 were applied only when there were sufficient data at appropriate conditions to perform the fit described. In many cases, especially for fuels at $\phi > 1.2$, cellularity occurred too early to allow for such a fit. In such cases laminar burn rate was determined using,

$$u_l = u_{n,\min}$$
(9)

where $u_{n,min}$ is the stretched, minimum burn rate experimentally measured, excluding the spark affected region of 0 ~ 8 mm in mean flame radius. Note that $u_{n,min}$ refers to an entrainment of unburned gas.

The approach followed for determination of the mean flame radius of turbulent flames is similar to that described above for laminar flames. The turbulent flame speed is given by,

$$S_{te} = \frac{dr_{sch}}{dt}$$
(10)

Here, r_{sch} is a mean flame radius based on the projected flame area, A_{sch}, while the subscript "e" denotes that the flame speed is based on an entrainment of unburned gas. The entrainment turbulent burning velocity, u_{te}, can then be determined by accounting for the expansion of the burned gas,

$$u_{te} = \frac{\rho_b}{\rho_u} \frac{dr_{sch}}{dt} = \frac{\rho_b}{\rho_u} S_{te}$$
(11)

For turbulent spherical flames, the effective thermal expansion ratio is increasing with flame size [13], however, accurate experimental determination of this effect requires large number of repeated tests. As the aim of the present work is comparative analysis of the different fuels, consistent application of Eq. 11 to the different conditions

studied is expected to reveal the sought tendencies, although the reported values of the burn rate might not admit direct comparison to alternative definitions.

3. Results and Discussion

3.1 Laminar Burning Velocity

Laminar burning velocity results for the fuels are displayed in Figure 3. The curves are 3rd order polynomial fits to the experimental data. Solid lines refer to results obtained via Eq. 7. Dotted lines correspond to u_l values computed using $u_l = u_{n,min}$. Rich flames for the fuels examined showed signs of cellularity as early as a mean flame radius of 8 mm. Consequently, too few data points were available to determine L_b. Burning velocities obtained in this way cannot be considered to be rigorously defined but represent a pragmatic approach to obtaining laminar burning velocity data to aid the analysis of subsequent turbulent burning measurements. Also included in the results of Figure 3 are indicative error bars. For $\phi \leq 1.1$ the uncertainty is that typical of schlieren imaging processing using the methods detailed above. For $\phi > 1.1$, the errors bars also reflect the statistical ambiguity induced by setting $u_l = u_{n,min;}$ their estimation involved extrapolation of the measured L_b values (Fig. 4) to the richest ϕ studied.

The u_l peaked close to $\phi = 1.1$ and demonstrated a dependence on molecular structure that was similar at all ϕ explored. Overlaps in burn rate ranking were evident only in the richest mixtures, where the impact of cellularity is greatest and consequent uncertainty in measured burn rate values the largest. The unsaturated fuels ranked top in u_l (1-hexyne > cyclohexene > 1-hexene), followed by cyclohexane and n-hexane. The branched alkanes burned slowest, with the double branched 2,2 dimethyl butane

being slower than the single branched isohexane. Similar rankings in laminar burn rate were reported in [4], from pressure-based analyses in a spherical bomb at initial conditions of 450 K and 0.3 MPa.

The Markstein length (L_b) of a flame is a physico-chemical flame parameter, customarily used to characterise the effect of stretch rate on flame speed [11]. Displayed in Figure 4 are measured (symbols, solid line fits) and extrapolated L_b values (dashed lined, used solely for u_l uncertainty estimates) for all fuels studied. Although of notable scatter, with COV as high as 25% [14], differences in the experimentally measured L_b for the different fuels (at fixed ϕ) were small, with the overall trend being a decrease in L_b with ϕ. This similarity in L_b for the various fuels can be attributed to their comparable thermo-diffusive characteristics, arising from their similar molar mass.

The experimentally measured values of u_l, were compared with computations from the Premix code of the CHEMKIN package [15], at the same unburned temperature and pressure (Figure 5). Data presented here are for n-hexane and cyclohexane, as these were the only two, out of the seven fuels studied, available in the code. Multi-component formulation for transport properties including Soret diffusion were used. The JetSurF 2.0 mechanism [16] was selected as it has been previously compared with laminar burning measurements at elevated conditions [4] and enabled comparison with a single mechanism. The agreement between the experiments and model at lean ϕ is good. Beyond $\phi = 1$ the flames were cellular from ignition so the experimental data corresponds to the minimum burning velocity recorded. It is to be expected that cellularity increases the burn rate [11], so it may explain why the measured values at $\phi > 1$ are higher than the computed values. The comparison is to some extent irrelevant, as flames of C_6 hydrocarbons do not exist as a single

uninterrupted flame front under rich conditions at the *Ti* and *Pi* studied here, since thermo diffusive effects result in localized quenching of the flame surface [11] very early during flame development. Hence, the computed u_l values could provide a useful, unambiguously defined reference, albeit they cannot be experimentally realised.

The development of hydrocarbon kinetic mechanisms has occurred rapidly in the previous few decades and this, allied with improvements in experimental methods for the determination of u_l has resulted in better understanding of the key molecule breakdown processes taking place within the flame. Based on the suggestions of previous workers [4-5, 17-19], main reasons for the differences in u_l are given below.

1. Unsaturated hydrocarbons have higher burning velocities than saturated hydrocarbons. This is to a degree attributed to their notably higher adiabatic flame temperatures, T_{ad} [2], owing to the high energy of their double or triple bond. For instance, thermodynamic equilibrium computations suggest that the T_{ad} of 1-hexyne is 5% higher c.f. that of n-hexane at lean mixtures and up to 10% higher at the extreme rich condition examined. The higher flame temperature accelerates transport processes at the flame front; following the kinetic theory of gases [20], the thermal diffusivity increases as the ~0.8 power of temperature and the molecular diffusivity of species increases as the ~1.65 power of temperature. From a kinetics point of view, it is implicit that a lower proportion of H atoms available in the "radical pool" formed during oxidation leads to a weaker propensity for chain branching reactions to boost burn rate [4-5, 17-18], in particular for the critical branching reaction $H + O_2 \rightarrow OH + O$. Hydrogen atoms are more easily abstracted from unsaturated molecules (i.e. 1-hexyne, 1-hexene, cyclohexene) due to the presence of the

relatively weaker allylic C-H bond ($\Delta H^o \sim 360$ kJ/mol); this promotes an additional, kinetic, advantage to the effect of their higher T_{ad}. There is also a larger number of combustion routes during break-down of alkenes/alkynes passing via ethyl radicals, leading to the production of extremely fast burning intermediate species, such as ethylene, vinyl radical and acetylene [4].

2. Branched alkanes burn slower than their straight chain equivalent. In the case of C_6 branched molecules (i.e. 2,2 dimethyl butane and 2-methyl pentane), the lack of long chain sites leads to the production of more, relatively non-reactive CH_3 radicals compared to n-hexane or cyclohexane oxidation, which contributes to a reduction in the overall burn rate [4, 18]. The lower ul of the branched alkanes can also be related to the propensity of hydrogen atom abstraction during oxidation. For example, in the case of 2,2 dimethyl butane, four out of the six carbon atoms constitute methyl groups with strong primary C-H bonds ($\Delta Ho \sim 425$ kJ/mol), with only one methylene group, possessing weaker secondary C-H bonds ($\Delta Ho \sim 410$ kJ/mol). Particularly for 2,2 dimethyl butane, C atom number two is attached to no H atoms, arguably further increasing the propensity of 2,2 dimethyl butane to produce CH_3 c.f. more reactive H radicals upon combustion. Conversely, 2-methyl pentane (isohexane) contains three methyl groups, two methylene groups and one methine group with a weaker tertiary C-H bond ($\Delta Ho \sim 405$ kJ/mol) and therefore has a slightly higher burning velocity than 2,2 dimethyl butane.

3. Ring molecules were found to burn generally faster than their straight chain counterparts. Cyclohexane was slightly faster than n-hexane, while the difference in laminar burn rate between cyclohexene and 1-hexene was even more prominent. This could be attributed to the ease of abstraction of

hydrogen radicals during the initial step of cyclohexane (C-H bonds are all secondary) and cyclohexene (only secondary and four weaker allylic C-H bonds) oxidation, which promotes chain branching before ring opening. Conversely, n-hexane and 1-hexene contain less sites with secondary and/or allylic C-H bonds.

3.2 Turbulent Burning Velocity

Contours of flame edge at 1.1 ms intervals generated from schlieren images of lean and rich turbulent n-hexane-air flames (ϕ = 0.78 and 1.17) are presented in Figure 6. As noted by previous workers there are observable differences in the way in which flames of different ϕ propagate [21]. The lean flames can be seen to be distorted by the turbulent flow field (i.e. local protrusions and recesses). This is in contrast to the development of rich flames which propagated outwards in a more uniform manner. Experimental turbulent burning velocities, $u_{te,}$ derived from the schlieren films are plotted against flame radius and shown in Figure 7, for n-hexane-air mixtures at ϕ = 0.98. Turbulent flames continuously accelerate from ignition. There are several factors contributing to this acceleration [13, 22-24]. The first factor is the growing effective thermal expansion ratio, because the average density behind the leading edge of a turbulent flame progressively decreases with growing flame brush thickness. The flame brush thickness has been shown to increase with flame radius [22]. The second factor is the increasing fraction of turbulent eddies smaller than the flame that can wrinkle the flame, increasing its surface area and, hence, its burn rate [23-24]. Finally, there is an increase in effective turbulent diffusion through a surface, the curvature of which is decreasing. As stated in the introduction, among the primary aims of this work was to compare the turbulent burn rates of different fuel-air mixtures, with

turbulent flames growing in a closed volume and accelerating, where the rate of acceleration is a function of turbulence [25] and to a lesser extent laminar flame speed [26]. In order to achieve a consistent comparison it was necessary to define the burning velocity and an appropriate point of comparison.

In this study, the turbulent burning velocity derived from schlieren measurements was defined as the entrainment turbulent burning velocity, u_{te} (Eq. 11). This definition has been compared to other definitions obtained via pressure recordings or laser sheet measurements [27]. With suitable post processing, it is possible to obtain alternatively defined burning velocities, however this is avoided here, as it not within the scope of the work and runs the risk of propagating errors.

All turbulent burning velocity comparisons were made at a flame radius, $r_{sch} = 30$mm. This radius was selected to be sufficiently large to ensure that there was no residual consequence of the initiation spark energy [28]. Comparison of turbulent burning velocities at a fixed flame size may result in uncertainties, as the selected radius was not attained at the same dimensionless time (e.g. time from ignition divided by integral time scale). Because the turbulent flow properties are fixed for comparison, differences in time taken for flames to propagate across the vessel arise from different u_l and in particular ρ_b / ρ_u. At a flame radius of $r_{sch} = 30$ mm, each flame would have experienced more than one integral length scale of $L = 20$ mm [29] and it would not have interacted with the fans. Following an approach used by previous workers [30], an effective rms turbulent velocity, u'_k can be found by integrating the turbulent power spectrum density and used to characterize turbulent flame development (the observed continuous increase in burn rate from ignition). For an infinitely large flame, $u'_k / u' = 1$, and the flame encompasses the entire spectrum of turbulent eddies. At $r_{sch} = 30$ mm, u'_k / u' was determined to be ~62% [14], thus an appreciable proportion of the

turbulent flow field has interacted with the flame. It has been shown that ranking fuels with respect to u_{te} at r_{sch} = 30mm is representative of their ranking at any other radii for 30 mm < r_{sch} < 65 mm [14]. Hence, qualitative trends with fuel type at r_{sch} = 30 mm are considered representative of the behaviour of the different flames at any other flame radii for the given apparatus.

Turbulent burn rate results at u' = 2 and 6 m/s are shown in Figure 8. The curves are 3rd order polynomial fits to the experimental data. The experimental scatter in u_{te} was ~10% COV and proved independent of u'. This was in accordance with previous measurements in this vessel [21]. Turbulence significantly enhanced the burn rate of all the fuels examined. To provide an overall trend for all the fuels studied, the average ratio of u_{te} / u_l was measured to be circa 3.5 and 7.5 at the leanest and richest mixtures explored for u' = 2 m/s. The corresponding values for u' = 6 m/s were about 7.0 and 18.0. Fastest laminar flames were observed at ϕ ~ 1.1 (Fig. 3). At moderate turbulence of u' = 2 m/s, the maximum burn rate, $u_{te,max}$, occurred at ϕ ~ 1.3. Stronger turbulence of u' = 6 m/s, yielded even larger displacement of $u_{te,max}$ towards rich conditions, at ϕ ~ 1.4. This trend is consistent with findings in [21].

The results of Figure 8 suggest that the influence of fuel molecular structure noted for laminar flames carried over to turbulent flames. Ranking between the fuels in terms of turbulent burn rate generally resembled that under laminar conditions. The unsaturated fuels ranked at the top, with 1-hexyne remaining the fastest, the branched fuels at the bottom, with 2,2 dimethyl butane remaining the slowest, and n-hexane remained intermediate. Cyclohexane was an exception to the trend, particularly so at u'= 2 m/s; however, the magnitude of the observed differences was not large and, arguably, the behaviour of cyclohexane could be attributed to the statistical accuracy of the measurements. In order to examine the relative differences between the fuels,

results have also been plotted with reference to the burning velocity of n-hexane in Figure 9. The decision to use n-hexane as the reference was based on the following criteria; a) it was considered the "base" fuel of the C_6 group, since it has a simple straight chain structure and no unsaturated bonds and b) its burn rate was average, hence it provides a better illustration of the prominent effects of branching (negative) and unsaturation (positive) on turbulent burn rate. In order to highlight the statistical trend observed, also included in the plots of Figure 9 are coefficients of variance (%) between the burn rates of the various fuels at each condition (flow and equivalence ratio). It was found that the difference between the burn rate of n-hexane and that of ring alkanes or 1-hexene remained around 5% to 10% at all ϕ explored and irrespective of whether the unburned mixture was laminar or turbulent. In contrast, the difference in the burn rate of n-hexane and that of the fastest (1-hexyne) and slowest fuels (branched alkanes) generally increased with turbulence under lean conditions and decreased with turbulence under rich conditions. This suggested that the magnitude of u_l became less influential under turbulent, fuel rich burning.

Laminar flamelets have been observed up to high levels of turbulence. In his review Driscoll [31] suggested that there was experimental evidence for the existence of flamelets for Karlovitz Numbers exceeding 10. Here, the Karlovitz number was defined as:

$$Ka = \left(\frac{u^{'}}{u_l} \right)^{3/2} \left(\frac{u_l L}{\alpha_0} \right)^{-1/2} \left(\frac{(T_p + T_R)/2}{300\,K} \right)^{1/2} \tag{12}$$

Where, α_0 is the diffusivity of nitrogen at 300 K, which is equal to 0.15 cm^2/s, and T_P and T_R are the temperatures of the reactants and products. In this study Ka varied between 1 and 4 for u' =2 m/s and 5 and 20 for u' = 6 m/s. Thickening of the preheat zone has been observed for lean propane flames, this has been attributed to response

of the flame to the net strain rate within the fluid [31], therefore, the flames studied here at lean equivalence ratios may be experiencing broadening on the preheat zone. This impacts on the flames to different degrees; for example, the unsaturated molecules in which hydrogen atoms are more easily abstracted were measured to be less affected than the branched ones. For rich equivalence ratios (for hydrocarbon fuels heavier than propane) thermodiffusive effects have been demonstrated, resulting in flamelet thickening and localized extinction in areas of negative curvature. In the current study, at rich ϕ conditions the relative differences between the fuels generally decreased; perhaps, the diffusion processes that depend on the mass of the molecule become more important.

There are a number of simple expressions for turbulent burn rate, used as sub-models in more complex models, which are able to represent the combustion chamber geometry. An example is the Zimont-Lipatnikov model [32], included in the computational fluid dynamics packages, ANSYS-FLUENT and CD-Adapco Star-CCM+. Some of these expressions use a power law format, where each of the significant parameters are expressed in the form $u_t = f(u_l^a, u'^b, \ldots)$. Using the results presented here, the effect of modifying u_l on u_{te} can be tested, whilst all other parameters are constant i.e. u', L_b, L. Shown in Figure 10 are values of u_{te} log plotted against u_l. The data are subdivided into groups of constant u' and ϕ and contain information for each of the fuels tested. Linear fits are shown for each group and represent fits of the form $u_{te} \propto u_l^n$. There is significant influence of the equivalence ratio. At the leanest mixtures, u_{te} markedly increased with u_l. For the richest mixtures, changes in u_l had lesser impact on u_{te}.

Plotted in Figure 11 are values of n vs ϕ for both u' examined. The magnitude of n was largest at the leanest conditions explored and decreased as the mixtures became

richer. There was a distinctive shift in the slope of n vs ϕ for rich conditions; n continued to decrease with increasing ϕ, albeit at a slower rate. The trend observed here resembles that observed in L_b. Thus the turbulent burn rate of leanest stretch sensitive flames is most sensitive to changes in the laminar burn rate. Rich thermo-diffusively unstable flames are relatively less sensitive to changes in u_l associated with different fuels.

4. Conclusions

The turbulent burning velocity remains a relatively poorly quantified parameter. The competing influence of the flame and flow field properties results in variation in experimental and modelled measurements. The result is that the impact of changing the fuel on the turbulent burning velocity cannot be predicted with certainty. Here the burn rate of premixed turbulent flames of hydrocarbon molecules consisting of six carbon atoms have been measured in a spherical fan stirred combustion vessel. Tests have been performed for equivalence ratios of ϕ = 0.78 to 1.65, at two rms turbulent velocities, u' = 2 and 6 m/s. To aid in the interpretation of the turbulent results the laminar burning velocity was also determined from filming of spherical expanding flames within the vessel. The results are expressed in the form of the turbulent burning velocity plotted against equivalence ratio, ϕ, at a mean flame radius of 30 mm. This approach builds on previous studies [14, 33] where it was found to be successful at illuminating the differences between fuels, which tend to be most marked for rich and lean flames.

- The unsaturated fuels 1-hexyne (triple C≡C bond) and cyclohexene (double C=C and ring structure) had the highest u_l. Ranking of the remaining fuels was: 1-hexene (unsaturated, double C=C bond), cyclohexane (unsaturated,

ring structure) and n-hexane (saturated). The iso-alkanes burned slowest, with the double branched 2,2 dimethyl butane being noticeably slower than the single branched 2-methyl pentane. This is in agreement with findings reported in [4].

- The measurements of Markstein Length, L_b, were highly scattered. However, no significant differences in L_b were observed. This similarity in L_b for the various fuels can be attributed to their similar thermo-diffusive characteristics, arising from their close molar mass.

- Turbulence increased the burn rate. As an average between all the fuels studied, for $u'= 2$ m/s the burn rate was increased by factors of 3.5 and 7.5 at the leanest and richest mixtures explored c.f. laminar conditions. The corresponding burn rate enhancement for $u'= 6$ m/s was 7.0 and 18.0.

- Turbulence shifted the equivalence ratio at which peak burn rates were attained towards richer mixtures. For all fuels studied, laminar burn rate peaked at $\phi \sim 1.1$; turbulent burn rate peaked at $\phi \sim 1.3$ for moderate turbulence of $u'= 2$ m/s and at $\phi \sim 1.4$ for stronger turbulence of $u'= 6$ m/s.

- At both turbulent intensities studied, the turbulent burn rates followed the same qualitative trends and rankings as for u_l. At $\phi = 0.78$ the difference between the fastest fuel, 1-hexyne, and slowest fuels, iso-hexane and 2,2 dimethylbutane, increased with u'. In contrast, at other equivalence ratios, the relative differences between the fuels decreased as u' increased indicating that the magnitude of the laminar burning velocity, u_l, becomes less influential, particularly so at rich ϕ.

- The turbulent burning velocity of lean, stretch sensitive flames is most sensitive to changes in the laminar burning velocity. Rich thermo-diffusively

unstable flames are relatively less sensitive to changes in u_l associated with different fuels.

Acknowledgements

References

[1]   Heywood, J.B., **Internal Combustion Engine Fundamentals, International Edition**, Mc Graw Hill, 1988, ISBN 0071004998

[2]   Davis, S.G., Law, C.K., **Determination of and Fuel Structure Effects on Laminar Flame Speeds of C1 to C8 Hydrocarbons**, Combust Sci Technol 140 (1998) 427

[3]   Beeckmann, J. Cai, L., Pitsch, H., **Experimental investigation of the laminar burning velocities of methanol, ethanol, n-propanol, n-butanol at high pressure,** Fuel 117 (2014) 340

[4]   Farrell, J.T., Johnston, R.J., Androulakis, I.P., **Molecular Structure Effects On Laminar Burning Velocities At Elevated Temperature And Pressure**, SAE Tech Paper (2004) 01-2936

[5]   Wu, F., Kelley, A.P., Law, C.K., **Laminar flame speeds of cyclohexane and mono-alkylated cyclohexanes at elevated pressure**, Combust Flame 159 (2012) 1417

[6]   Comandini, A., Dubois, T., Chaumeix, N., **Laminar flame speeds of n-decane, n-butylbenzene, and n-propylcyclohexane mixtures**, Proc Comb Inst 35 (2015) 671

[7]   Vollhardt, P., Schore, N., **Organic Chemistry: Structure and Function, 6th Edition**, W.H. Freeman Publishers, 201, ISBN 142920494X

[8]   Burluka, A.A., Gaughan, R.G., Griffiths, J.F., Mandilas, C., Sheppard, C.G.W., Woolley, R., **Turbulent Burning Rates of Gasoline Components, Part 1 - Effect of Carbon Number**, Fuel, xxx (2015), xxx, in press

[9]   Gillespie, L., Lawes, M., Sheppard, C.G.W., Woolley, R., **Aspects of Laminar and Turbulent Burning Velocity Relevant to SI Engines**, SAE Tech Paper (2000) 2000-01-0192

[10]   Bradley, D., Hicks, R.A., Lawes, M., Sheppard, C.G.W., Woolley, R., **The measurement of laminar burning velocities & markstein numbers for i-octane–air and i-octane–n-heptane–air mixtures at elevated T and P in an explosion bomb**, Combust Flame 115 (1998) 126

[11]   Bradley, D., Sheppard, C.G.W., Woolley, R., Greenhalgh, D.A., Lockett, R.D., **The development and structure of flame instabilities and cellularity at low Markstein numbers in explosions**, Combust Flame 122 (2000) 195

[12]   Kelley, A.P., Smallbone, A.J., Zhu, D.L., Law, C.K., **Laminar flame speeds of C5 to C8 n-alkanes at elevated pressures: Experimental determination, fuel similarity, and stretch sensitivity**, P Combust Inst 33 (2011) 963

[13]   Lipatnikov, A.N., Chomiak, J., **Transient and Geometrical Effects in Expanding Turbulent Flames**, Combust Sci Technol 154 (2000) 75

[14]   Mandilas, C., "**Laminar and turbulent burning characteristics of hydrocarbon fuels**", PhD Thesis, University of Leeds, 2008

[15]   Kee, R.J., Grcar, J.F., Smooke, M.D., Miller, J.A., **A FORTRAN Program for Modeling Steady Laminar One-dimensional Premixed Flames**, SAND85, Sandia National Lab., 1985

[16]   Wang, H., Dames, E., Sirjean, B., Sheen, D.A., Tango, R., Violi, A., Lai, J.Y.W., Egolfopoulos, F.N., Davidson, D.F., Hanson, R.K., Bowman, C.T., Law, C.K., Tsang, W., Cernansky, N.P., Miller, D.L., Lindstedt, R.P, **A high-temperature chemical kinetic model of n-alkane (up to n-dodecane), cyclohexane, and methyl-, ethyl-, n-propyl and n-butyl-cyclohexane oxidation at high temperatures**, JetSurF version 2.0, September 19, 2010

[17]   Dryer, F.L., Westbrook, C.K., **Chemical kinetic modeling of hydrocarbon combustion**, Prog Energ Combust 10 (1984) 1

[18]   Johnston, R.J., Farrell, J.T**., Laminar burning velocities and Markstein lengths of aromatics at elevated temperature and pressure**, P Combust Inst 30 (2005) 217

[19]   Glassman, I., Yetter, R.A., **Combustion, 4th Edition**, Academic Press, 2008, ISBN 0120885735

[20]   Bird, R.B., Stewart, W.E., Lightfoot, E.N., **Transport Phenomena, Revised 2nd Edition,** John Wiley & Sons, 2007, ISBN 0470115394

[21]   Lawes, M., Ormsby, M.P., Sheppard, C.G.W., Woolley R., **The turbulent burning velocity of iso-octane/air mixtures**, Combust Flame, 159 (2012) 1949

[22]   Burluka, A.A., Hussin, A.M.T.E., Sheppard, C.G.W., Liu, K., Sanderson, V., **Turbulent Combustion of Hydrogen-CO Mixtures**, Flow Turbul Combust 86 (2011) 735

[23]   Lipatnikov A.N., Chomiak J., **Molecular transport effects on turbulent flame propagation and structure**, Prog Energ Combust Sci 31 (2005) 1

[24]   Lawes, M., Ormsby, M.P., Sheppard, C.G.W., Woolley, R., **Variation of turbulent burning rate of methane, methanol, and iso-octane air mixtures**

with equivalence ratio at elevated pressure, Combust Sci Tech 177 (2005) 127

[25] Borghi, R., **Turbulent combustion modelling**, Prog Energ Combust 14 (1988) 245

[26] Zimont, V.L., **Gas premixed combustion at high turbulence, turbulent flame closure combustion model**, Exp Therm Fluid Sci 21 (2000) 179

[27] Bradley, D., Haq, M.Z., Hicks R.A., Kitagawa T., Lawes M., Sheppard, C.G.W. and Woolley R., **Turbulent burning velocity, burned gas distribution, and associated flame surface definition**, Combust Flame 133 (2003) 415

[28] Bradley, D., Lung, F.K., **Spark ignition and the early stages of turbulent flame propagation**, Combust Flame 69 (1987) 71

[29] Nwagwe, K., Weller, H.G., Tabor, G.R., Gosman, A.D., Lawes, M., Sheppard, C.G.W., Woolley, R., **Measurements and Large Eddy Simulations of Turbulent Premixed Flame Kernel Growth**, P Combust Inst 28 (2000) 51

[30] Abdel-Gayed, R.G., Bradley, D., Lawes, M., **Turbulent burning velocities: a general correlation in terms of straining rates**, Proc R Soc Lond A414 (1987) 389

[31] Driscoll, J.F., **Turbulent premixed combustion: Flamelet structure and its effect on turbulent burning velocities**, Prog Energ Combust Sci 34 (2008) 91

[32] Lipatnikov, A.N., **Fundamentals of Premixed Combustion**, CRC Press, Boca Raton, 2013

[33] Mandilas, C. Ormsby, M.P., Sheppard, C.G.W., Woolley, R., **Effects of H_2 addition on laminar and turbulent premixed methane and iso-octane–air flames**, Proc Comb Inst 31 (2007) 1443
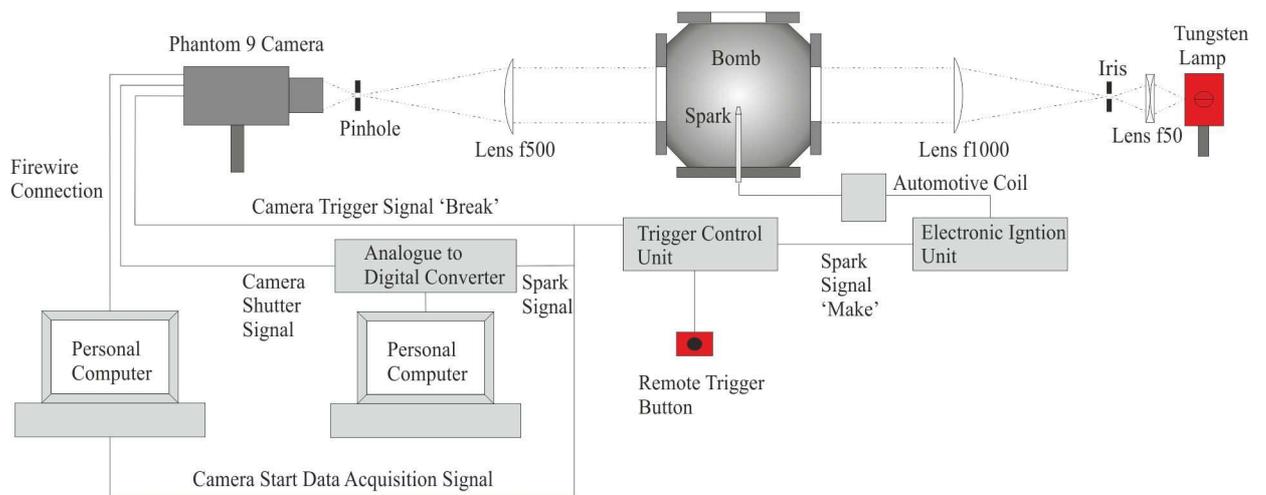
Figure 1 – Schematic of the DAQ for schlieren imaging of deflagrations inside the bomb.
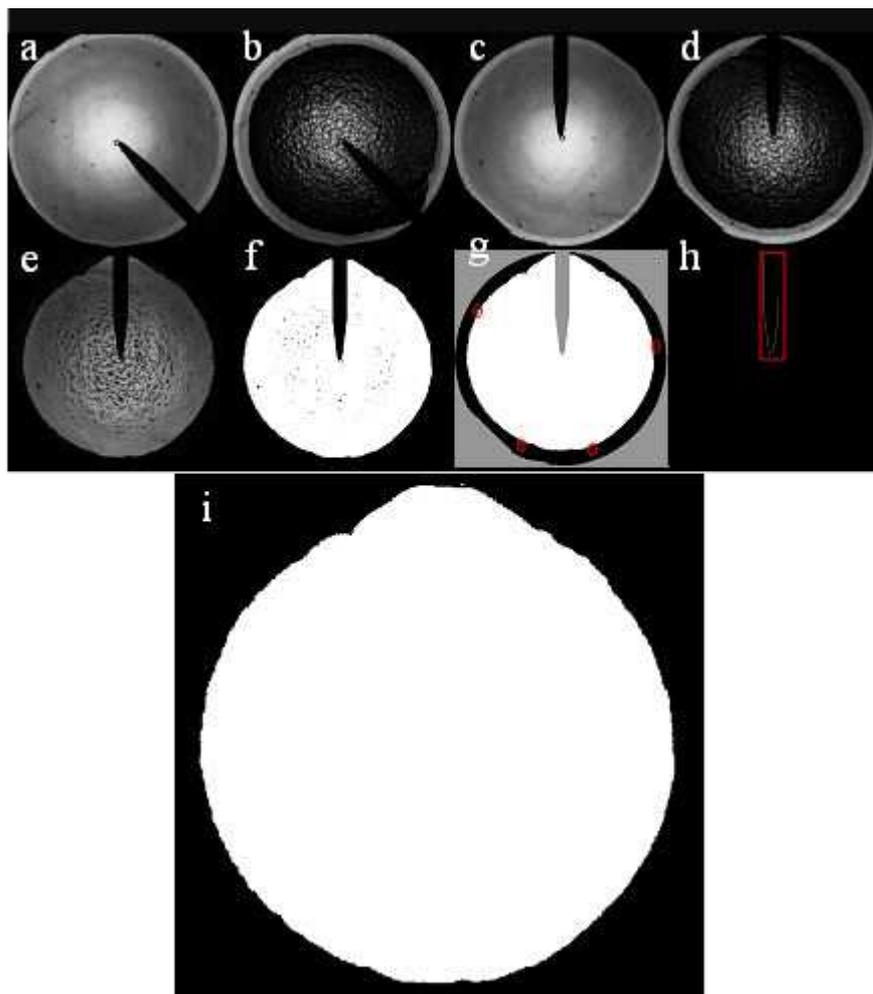
Figure 2 – Processing steps for a sample n-octane laminar stoichiometric flame; method of processing of flame images was the same regardless of the fuel type and conditions.
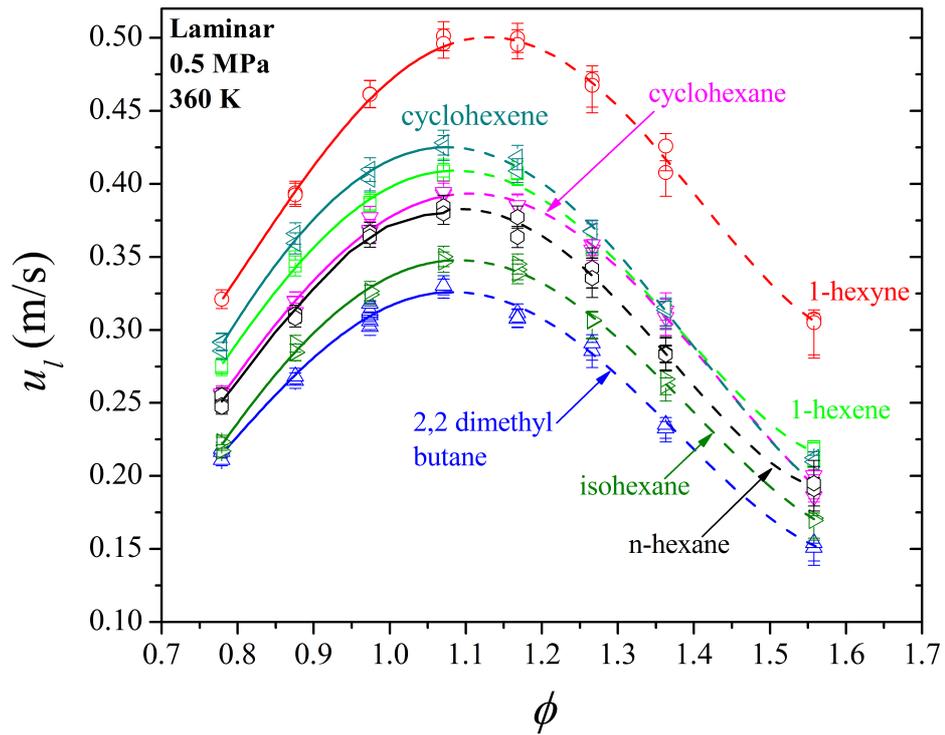
Figure 3 – Plots of stretch-free burning velocities against ϕ, obtained using Eq. 7. Initial pressure and temperature of 0.5 MPa and 360 K.
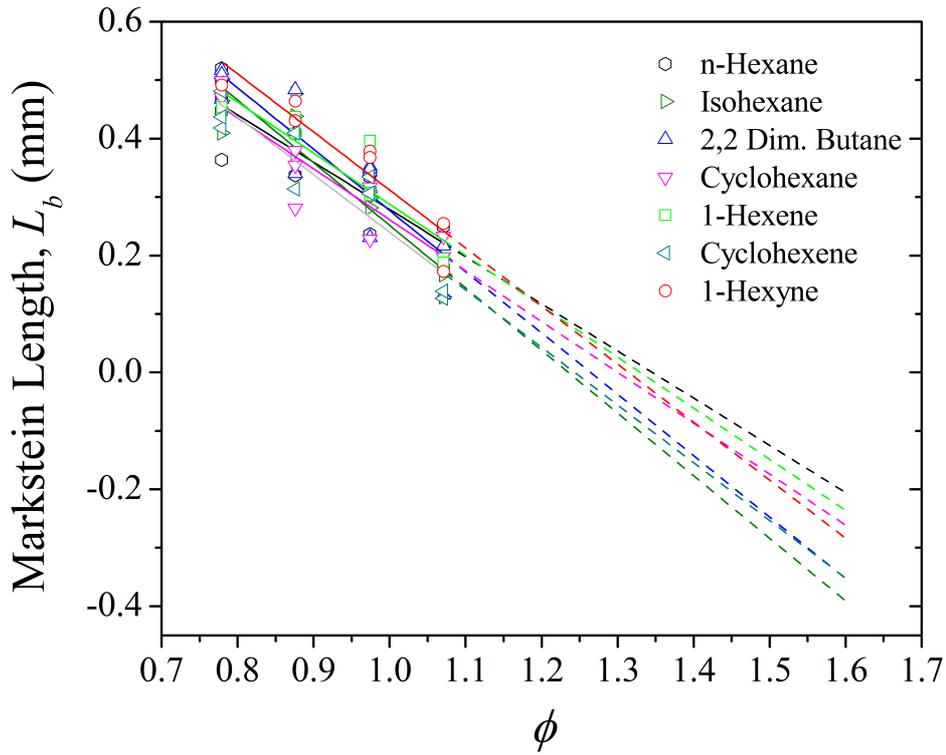
Figure 4 – Burnt Markstein lengths, L_b, obtained using Eq. 6 plotted against ϕ. Dashed lines reflect extrapolations from measurements.
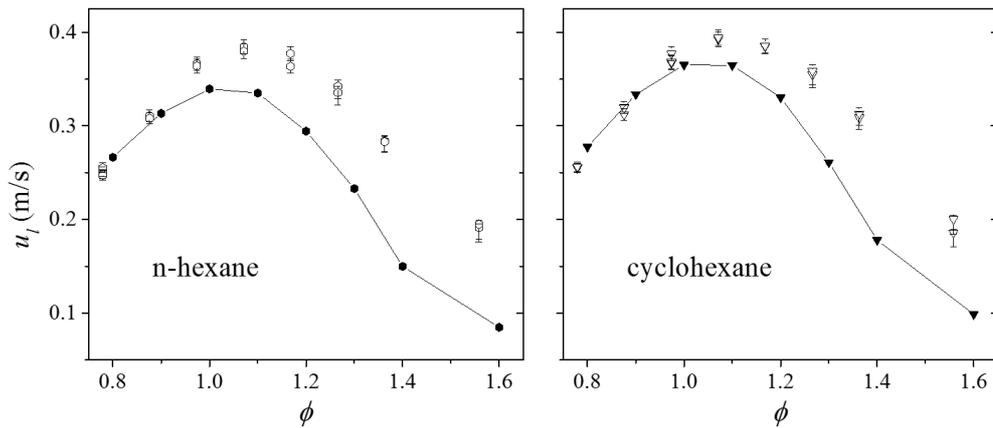
Figure 5 – Comparison of experimental burning velocity (open symbols) with numerical computations (filled symbols) performed with Jetsurf 2.0. Initial temperature and pressure of 360 K and 0.5 MPa.
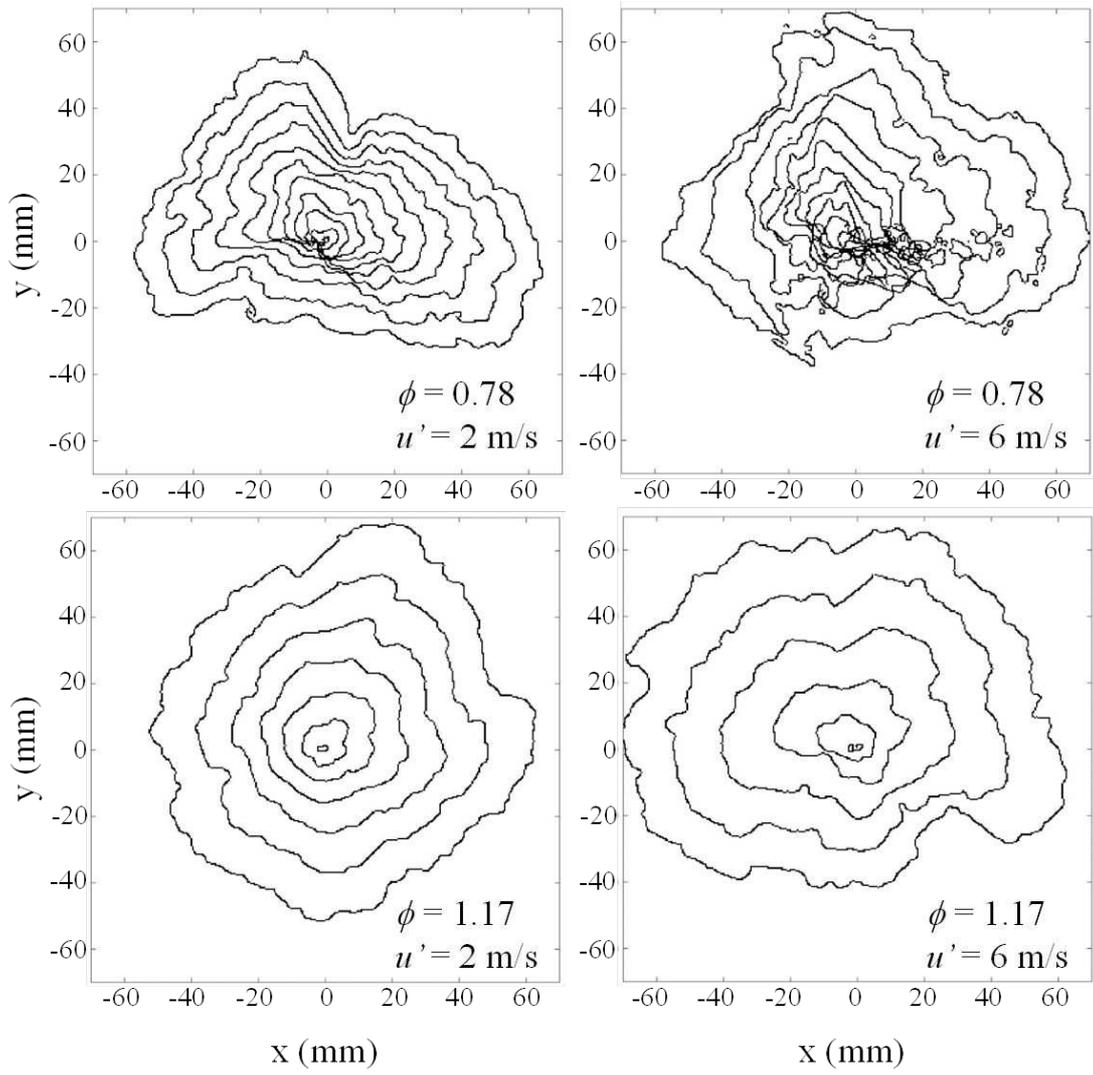
Figure 6 – Sample flame contours of turbulent n-hexane flames.
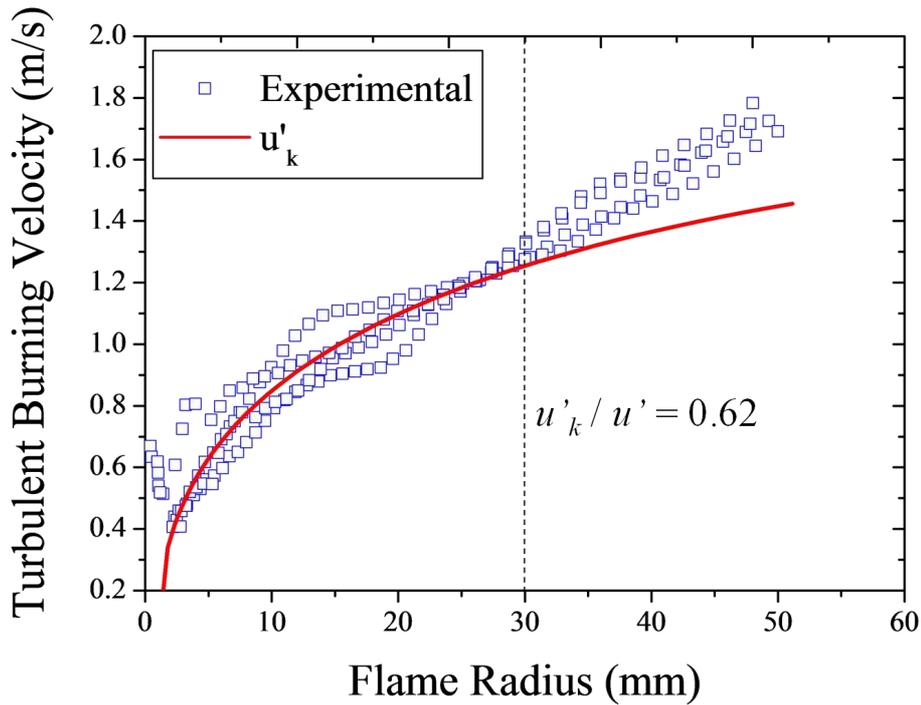
Figure 7 – Exemplar turbulent flame growth versus flame radius at $u' = 2$ m/s for n-hexane-air mixtures at $\phi = 0.98$, with initial pressure and temperature of 0.5 MPa and 360 K. The effective r.m.s turbulent velocity, u'_k is also shown.
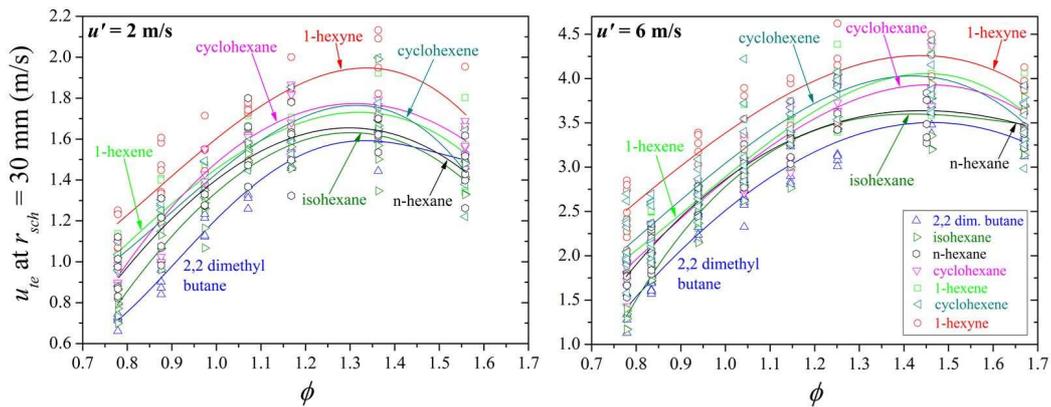
Figure 8 – Entrainment turbulent burning velocities at mean flame radii of 30 mm, plotted against ϕ. Initial pressure and temperature of 0.5 MPa and 360 K.
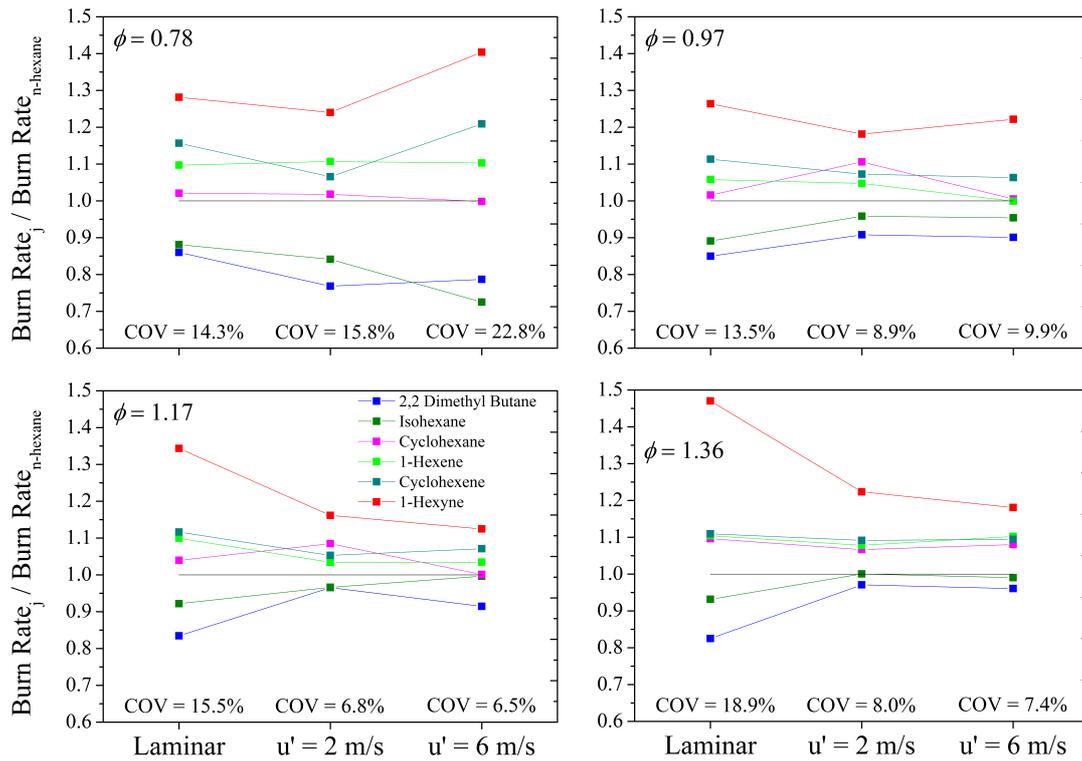
Figure 9 – Relative ratios in burning velocity, referenced against n-hexane, under laminar and turbulent conditions. Plots also include the percentile coefficient of variance between the burn rates of the various fuels at each condition. Averaged values were used.
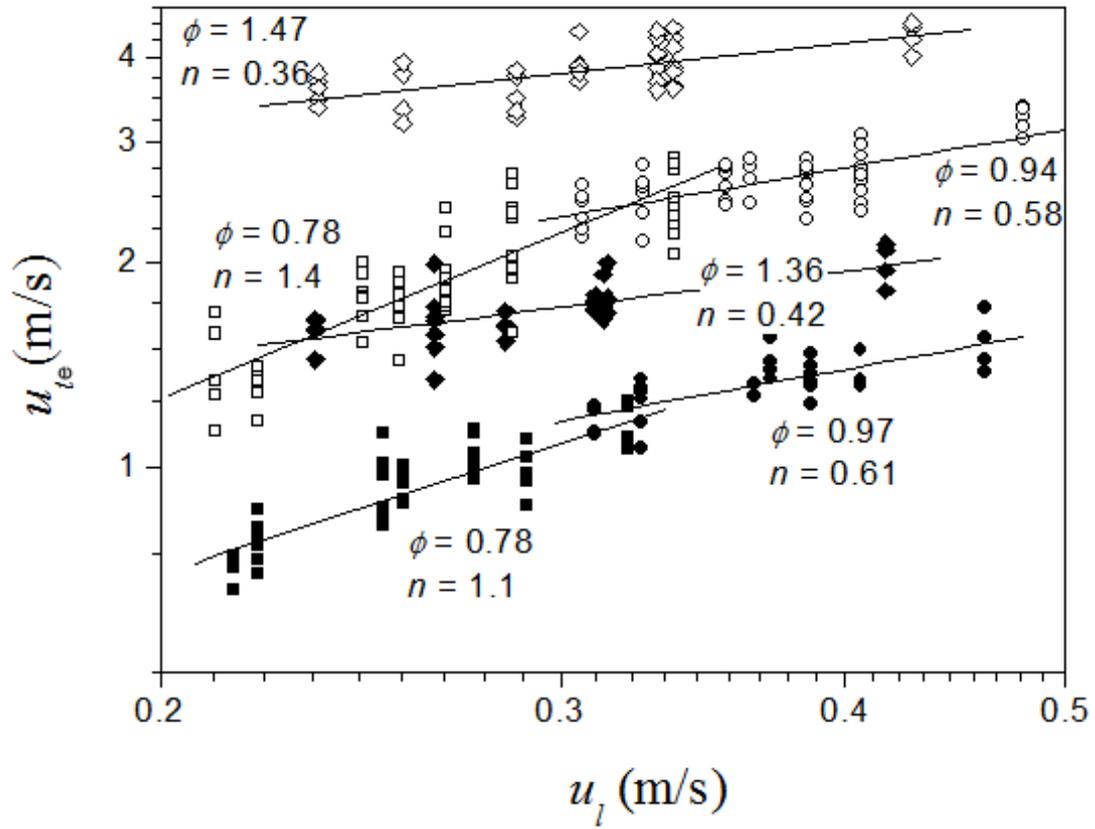
Figure 10. Values of u_t plotted against u_l. Filled symbols, $u' = 2$ m/s; open symbols, $u' = 6$ m/s. Each group is made up of data from different fuels at the same u' and ϕ. The gradients of the fits shown, given as n.
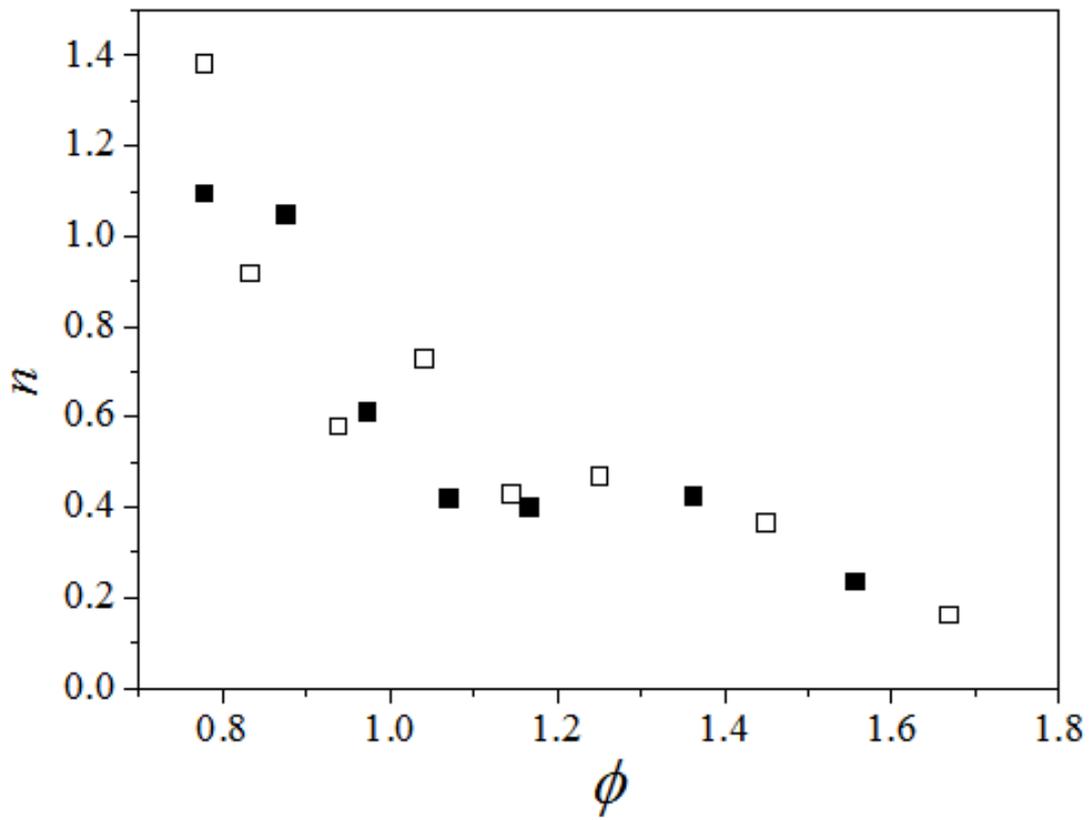
Figure 11. Values of the exponent, n where $u_{te} \propto u_l^n$. Filled symbols, $u' = 2$ m/s; open symbols, $u' = 6$ m/s.

Table 1 – Schematic diagrams showing structure and types of bonds in each molecule. Heat of formation, molar mass and bond strengths also included in the table. Bond strengths and heat of formation data were found in [7].

Fuel	2D Structure	Heat of Formation (kJ/mol)	Molar Mass (g/mol)	Colour Legend – Bond Strengths
2,2 Dimethyl Butane		-185.6	86.17	Primary C-H, $\Delta H° \sim 425$ kJ/mol; Secondary C-H, $\Delta H° \sim 410$ kJ/mol; Tertiary C-H, $\Delta H° \sim 405$ kJ/mol; Allylic C-H, $\Delta H° \sim 360$ kJ/mol; Vinylic C-H, $\Delta H° \sim 460$ kJ/mol; Acetylenic C-H, $\Delta H° \sim 550$ kJ/mol
2, Methyl pentane (isohexane)		-174.3	86.17	
n-Hexane		-167.1	86.17	
Cyclohexane		-124.6	84.16	Single C-C, $\Delta H° \sim 350$ kJ/mol; Double C=C, $\Delta H° \sim 620$ kJ/mol; Triple C≡C, $\Delta H° \sim 830$ kJ/mol
1-Hexene		-42	84.16	
Cyclohexene		-4.32	82.14	
1-Hexyne		122.3	82.14	

Fuel	2D Structure	Heat of Formation (kJ/mol)	Molar Mass (g/mol)	Colour Legend – Bond Strengths
2,2 Dimethyl Butane		-185.6	86.17	
2, Methyl pentane (isohexane)		-174.3	86.17	**Primary C-H, ΔH° ~ 425 kJ/mol** **Secondary C-H, ΔH° ~ 410 kJ/mol** Tertiary C-H, ΔH° ~ 405 kJ/mol Allylic C-H, ΔH° ~ 360 kJ/mol Vinylic C-H, ΔH° ~ 460 kJ/mol Acetylenic C-H, ΔH° ~ 550 kJ/mol
n-Hexane		-167.1	86.17	
Cyclohexane		-124.6	84.16	Single C-C, ΔH° ~ 350 kJ/mol Double C=C, ΔH° ~ 620 kJ/mol Triple C≡C, ΔH° ~ 830 kJ/mol
1-Hexene		-42	84.16	
Cyclohexene		-4.32	82.14	
1-Hexyne		122.3	82.14	